Astronomy & Astrophysics manuscript no. 11902rauer
September 18, 2009

Transiting exoplanets from the CoRoT space mission VII. The "hot-Jupiter"-type planet CoRoT-5b

Rauer, H.[1,2], Queloz, D.[3], Csizmadia, Sz.[1], Deleuil, M.[4], Alonso, R.[4], Aigrain, S.[5], Almenara, J.M.[6], Auvergne, M.[7], Baglin, A.[7], Barge, P.[4], Bordé, P.[16], Bouchy, F.[8], Bruntt, H.[9], Cabrera, J.[1], Carone, L.[10], Carpano, S.[11], De la Reza, R.[19], Deeg, H.J.[6], Dvorak, R.[12], Erikson, A.[1], Fridlund, M.[11], Gandolfi, D.[14], Gillon, M.[3,18], Guillot, T.[13], Guenther, E.[14], Hatzes, A.[14], Hébrard, G.[8], Kabath, P.[1], Jorda, L.[4], Lammer, H.[15], Léger, A.[16], Llebaria, A.[4], Magain, P.[18], Mazeh, T[20], Moutou, C.[4], Ollivier, M.[16], Pätzold, M.[10], Pont, F[5], Rabus, M.[6], Renner, S.[1], Rouan, D.[7], Shporer, A.[20], Samuel, B.[16], Schneider, J.[17], Triaud, A.H.M.J.[3], and Wuchterl, G.[14]

(Affiliations can be found after the references)

00 / 00

ABSTRACT

Aims. The CoRoT space mission continues to photometrically monitor about 12000 stars in its field-of-view for a series of target fields to search for transiting extrasolar planets ever since 2007. Deep transit signals can be detected quickly in the "alarm-mode" in parallel to the ongoing target field monitoring. CoRoT's first planets have been detected in this mode.
Methods. The CoRoT raw lightcurves are filtered for orbital residuals, outliers, and low-frequency stellar signals. The phase folded lightcurve is used to fit the transit signal and derive the main planetary parameters. Radial velocity follow-up observations were initiated to secure the detection and to derive the planet mass.
Results. We report the detection of CoRoT-5b, detected during observations of the LRa01 field, the first long-duration field in the galactic anti-center direction. CoRoT-5b is a "hot Jupiter-type" planet with a radius of $1.388^{+0.046}_{-0.047}$ R_{Jup}, a mass of $0.467^{+0.047}_{-0.024}$ M_{Jup}, and therefore, a mean density of $0.217^{+0.031}_{-0.025}$ g cm^{-3}. The planet orbits an F9V star of 14.0 mag in 4.0378962±0.0000019 days at an orbital distance of $0.04947^{+0.00026}_{-0.00029}$ AU.

Key words. planetary systems - techniques: photometry - techniques: radial velocity

[1]

1. Introduction

CoRoT started to search for the photometric signal of transiting extrasolar planets in 2007, after its successful launch in December 2006, for details on the satellite see the pre-launch book (Baglin et al. 2007; Boisnard et al. 2006) and Auvergne et al. (2009). The satellite monitors about 12000 stars per exoplanet field-of-view in a series of short (∼30 days) and long (∼150 days) observing runs. Its magnitude range is $12 \leq m_v \leq 16$ mag. The resulting stellar lightcurves are searched for periodic signals of transiting extrasolar planets. Radial-velocity follow-up measurements secure the nature of the transiting body and allow us to derive its mass.

The nominal lightcurve analysis for small transiting signals has to await the completion of an observing run and detailed signal analysis. The mission "alarm-mode" (Quentin et al. 2006; Surace et al. 2008), however, can be used to quickly trigger follow-up measurements during ongoing observations of a target field. The "alarm-mode" is used to increase the transmitted time-sampling for individual stellar lightcurves in the CoRoT exoplanet channel. The sampling is increased from 512 sec to 32 sec if a transit-like signal is detected during the observations. It therefore provides planetary candidates early during an observing run, which are, however, biased towards relatively large planetary candidates because of the limited data set available at this point.

CoRoT-5b is the fifth secured transiting planet detected by CoRoT. As CoRoT-1b to CoRoT-4b (Alonso et al. 2008; Barge et al. 2008; Deleuil et al. 2008; Moutou et al. 2008; Aigrain et al. 2008), it was first detected by the alarm-mode. Here, we present the photometric detection of CoRoT-5b by the satellite based on pre-processed alarm-mode data, the accompanying radial-velocity observations confirming its planetary nature, and the resulting planet parameters.

2. Observations and data reduction

CoRoT-5b was detected in the LRa01-field, the second long-run field of CoRoT. The field is located near the anti-center direction of the galaxy at RA(2000): $06^h46^m53^s$ and DEC(2000): -00°12'00" (Michel et al. 2006). The observ-

[1] Observations made with SOPHIE spectrograph at the Observatoire de Haute Provence (07B.PNP.MOUT), France, and HARPS spectrograph at ESO La Silla Observatory (072.C-0488(E), 082.C-0312(A)), and partly based on observations made at the Anglo-Australian Telescope. The CoRoT space mission, launched on December 27, 2006, was developed and is operated by CNES, with the contribution of Austria, Belgium, Brasil, ESA, Germany, and Spain.

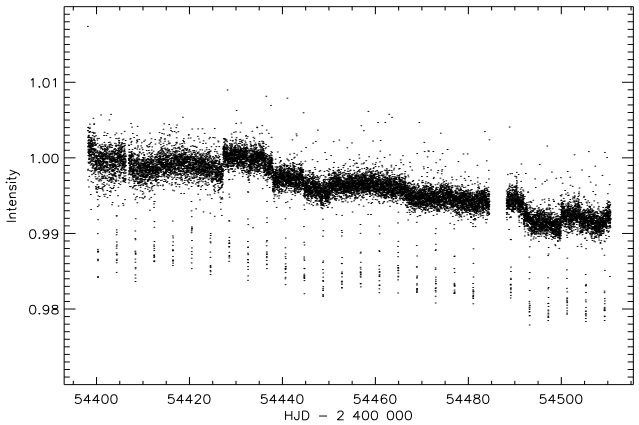

Fig. 1. Lightcurve of CoRoT-5 re-sampled to 512 sec time resolution. No corrections for data jumps due to "hot pixels" have been applied in this figure to show the raw data quality.

ing sequence started on October 24, 2007 and finished after 112 days duration. CoRoT observations usually have a very high duty cycle since data gaps are mainly caused by the regular crossings of the South Atlantic Anomaly (SAA), which typically last for about 10 min. During the observations of the LRa01 field, however, two longer interruptions occurred. An intermediate interruption of about 12 hours occurred eight days after the beginning of the observing run, and a longer data gap of about 3.5 days started on January 18, 2008, after a DPU reset. Finally, a duty cycle of 93 % was achieved.

The alarm-mode was triggered after 29 days of observations. When seven transit-like signals were detected, the time sampling was switched to 32 sec. The alarm-mode data for CoRoT-5 are based on the analysis of "white light" lightcurves, without using the color information of the CoRoT prism. In total 219,711 data points were obtained, 214,938 of it in oversampling mode. The data pipeline flags data points taken during the SAA crossing or affected by other events decreasing the data quality. When taking only unflagged data into account, the number of data points reduced to 204,092 in total and 199,917 as highly sampled.

The alarm-mode data were processed with a first version of the data reduction pipeline (Auvergne et al. 2009). The pipeline corrects for the CCD zero offsets and gain, the sky background intensity and the telescope jitter. In addition, "hot pixels" (Pinheiro da Silva et al. 2008) affect the lightcurves, causing sudden jumps in intensity of varying duration. The lightcurve of CoRoT-5 was, however, only moderately affected by such jumps, as can be seen in Fig. 1, which shows the full lightcurve. The oversampled part of the data set was re-binned to display the whole lightcurve with a 512 sec time sampling. The measured intensity decreases during the observing run, as observed for all stars in the fields. Overall, CoRoT-5 only shows a minor level of variability, without clear periodicity.

CoRoT measures stellar intensities by aperture photometry using optimized masks (Llebaria et al. 2003) that encompass the shape of the stellar point-spread-functions (PSFs). The bi-prism introduced in the light path of the exoplanet channel (Auvergne et al. 2009) causes relatively wide PSFs of unusual shapes that vary with e.g. stellar

Table 1. Radial velocity measurements of the star CoRoT-5 obtained by SOPHIE and HARPS spectrographs from December 2007 to December 2008.

BJD -2400000	RV $\mathrm{km\,s^{-1}}$	Error $\mathrm{km\,s^{-1}}$
SOPHIE		
54463.4939000	48.947	0.017
54465.5247100	48.816	0.028
54506.3770000	48.767	0.016
54525.3478500	48.860	0.020
54528.2886100	48.933	0.031
54544.3463300	48.925	0.026
HARPS		
54548.583775	48.933	0.014
54550.577783	48.792	0.021
54551.584161	48.865	0.013
54553.525234	48.883	0.010
54554.546158	48.819	0.012
54556.554191	48.929	0.010
54768.852140	48.820	0.009
54769.848137	48.900	0.008
54771.850953	48.851	0.009
54772.841289	48.827	0.010
54773.847921	48.900	0.008
54802.777527	48.929	0.009
54805.748602	48.852	0.012

magnitude. Contaminating eclipsing binary stars within the PSF could mimic a planetary transit-like signal. Based on the pre-launch observations of the target field included in the *Exo-Dat* data base (Deleuil et al. 2009), the contamination of the mask of CoRoT-Exo5 is estimated to 8.4 %. Refinement of this value will be performed in a more detailed future analysis using the dedicated windowing mask for this target star. We subtracted this flux level from the lightcurve before normalization to take low level contamination into account.

The overall intensity trend and smaller scale variability of the lightcurve were removed. To do this, we resampled the lightcurve to 512 seconds sampling rate first and convolved this lightcurve with a fourth order Savitzky-Golay filter (similar to the treatment for CoRoT-2b (Alonso et al. 2008)). Then median averages were calculated for 24 hour segments of the lightcurve (excluding the transit points and the data jumps), which was fitted by a spline-curve. The original lightcurve was then divided by the spline fit. The filtered lightcurve was used for normalization and further analysis. The out-of-eclipse scatter of CoRoT-5 was determined from the standard deviation of data points in the phase-folded lightcurve. It was found to be 0.0017 mag.

3. Photometric follow-up observation

Photometric follow-up observations with higher spatial resolution than CoRoT's (of $\approx 20''$x $6''$) are used to exclude the presence of nearby contaminating eclipsing binaries (Deeg et al., this volume). Such observations of CoRoT-5 were performed at the 80cm telescope at IAC, Tenerife, on the January 12, and March 11, 2008 at a spatial resolution of about $1.5''$. These data showed only one star bright enough to cause a potential false alarm, about $8''$ southwest of the target. Observations obtained during and out of a transit ("on/off photometry") showed, however, that

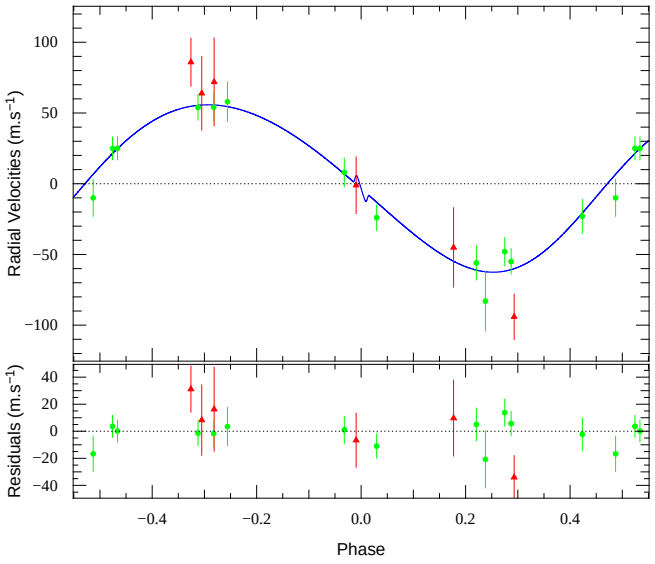

Fig. 2. Radial velocity measurements and Keplerian fit to the data including the Rossiter effect. Red: SOPHIE, green: HARPS.

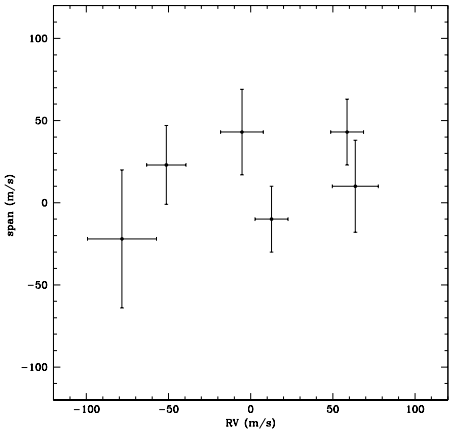

Fig. 3. Bisector analysis of CoRoT-5.

this contaminating star varies by less than 0.08 mag. This is far below the variation of about 0.55 mag that is required to explain the observed signal in the CoRoT data.

4. Radial velocity follow-up observations

In January 2008, after the identification of a transit signal by the alarm-mode, CoRoT-5 was observed with the SOPHIE spectrograph installed on the 193 cm telescope at the Haute Provence Observatory. Two radial velocity measurements were taken at opposite quadrature phases of the radial velocity variation expected from the transit ephemerides assuming a circular orbit. At this time the data were found to be compatible with a radial velocity amplitude suggesting a Jupiter mass planet. Additional measurements were obtained later in the season to confirm the reality of the signal but not enough to obtain a precise measurement of the orbit eccentricity. One year later, a new series of measurements was obtained with the HARPS spectrograph installed on the 3.6m ESO telescope at La Silla in Chile (Mayor et al. 2003). Both sets of data (SOPHIE and HARPS) have been processed as in Bouchy et al. (2008). Radial velocities (RV) were computed by weighted cross-correlation (Baranne et al. 1996; Pepe et al. 2005) with a numerical G2-spectral template excluding spectral orders below 4200 Å. Radial velocity values are listed in Table 1 and plotted in Fig. 2.

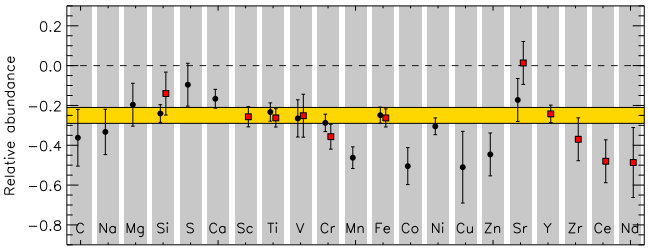

Fig. 4. Stellar abundances of CoRoT-5. Abundances found from neutral lines are marked by circles, for ionized lines box symbols are used.

We analyzed the cross-correlation function computed from the HARPS spectra using the line-bisector technique according to the description in Queloz et al. (2001) to detect possible spectral distortions caused by a faint background eclipsing binary mimicking a small RV amplitude signal. No correlation between the RV data and the bisector span was found at the level of the uncertainty on the data (Fig. 3).

The stability of the bisector, combined both with the amplitude of the radial velocity and the accuracy of transit lightcurve, is enough to discard an alternate background eclipsing binary scenario. In the case of a hypothetical background eclipsing binary, obtaining a sine-shaped radial-velocity signal would require a superimposed spectrum moving with the same systemic velocity as the brightest component, and on an RV range corresponding to the sum of the width of both CCF line profiles. This prerequisite constrains both on the mass of the potential eclipsing component and its companion. The example of HD41004 provides us with an interesting benchmark (Santos et al. 2002). This system was detected with a similar radial velocity amplitude but with a strong bisector correlation, and could be explained by a superimposed spectrum with 3% flux of the bright star. If one scales down this result to CoRoT-5, which has no bisector correlation, one finds that the contrast ratio between the brightest star and the hypothetical eclipsing binary is such that the eclipse must be very deep and the radius of the eclipsing stars much smaller than CoRoT-5. Considering the quality of the CoRoT lightcurve such a binary scenario does not match the transit ingress and egress timing and the detailed shape of the curve.

5. Properties of the central star

We determined the fundamental parameters of the host star carrying out a spectral analysis of the set of HARPS spectra acquired for radial velocity measurements. The individual

Table 2. Parameters of the parent star CoRoT-5.

parameter	value	source
RA	$06^h\ 45^m\ 07^s$	*Exo-Dat*
DEC	$00^\circ\ 48'\ 55''$	*Exo-Dat*
epoch	2000.0	
type	F9V	*Exo-Dat, AAOmega*
V	14.0	*Exo-Dat*
GSC2.3 ID	N82O011953	
2MASS ID	06450653+0048548	
$v \sin i$ [km s^{-1}]	1±1	VWA
ξ_t [km s^{-1}]	0.91±0.09	VWA
$T_{\rm eff}$ [K]	6100±65	VWA
$\log g$	4.19±0.03	VWA
$[M/H]$	-0.25 ± 0.06	VWA
M_{star} [$M_\odot$]	1.00±0.02	Evolut. tracks
R_{star} [$R_\odot$]	1.186±0.04	Evolut. tracks
$M^{(1/3)}/R$ [$M_\odot^{1/3}$ / $R_\odot$]	0.843±0.024	lightcurve
age [Gyr]	5.5 - 8.3	photometry +Evolut. tracks

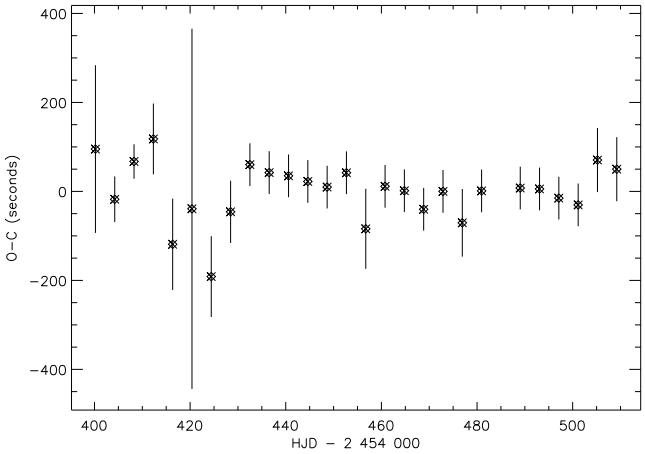

Fig. 5. The O-C diagram of the CoRoT-5b system. No clear period variation can be seen.

spectra were reduced with the HARPS standard pipeline. The extracted spectra were corrected for cosmics impacts, for the Earth and the stars velocity, and then corrected for the blaze function and normalized, order by order, to increase the signal-to-noise (S/N). The S/N level in the continuum is around 40 in the range 5 000-6 500 Å and it decreases to 15 towards the blue at 4 000 Å.

Spectroscopic observations of the central star have also been performed in January 2008 with the AAOmega multi-object facility at the Anglo-Australian Observatory. By comparing the low-resolution (R=1300) AAOmega spectrum of the target with a grid of stellar templates, as described in Frasca et al. (2003) and Gandolfi et al. (2008), we derived the spectral type and luminosity class of the star (F9 V).

As for the previous planet host stars, we used different methods to derive Corot-5 atmospheric parameters: line profile fitting with the SME (Valenti & Piskunov 1996) and the VWA packages (Bruntt et al. 2002, 2008). We find general agreement and here we quote the results from VWA. The star has a very low projected rotational velocity, $v \sin i = 1 \pm 1\,\mathrm{km\,s^{-1}}$. More than 600 mostly non-blended lines were selected for analysis in the wavelength range 3 990–6 810 Å. VWA uses atmosphere models from the grid by Heiter et al. (2002) and atomic parameters from the VALD database (Kupka et al. 1999). The abundance determined for each line is computed relative to the result for the same line in the solar spectrum from Hinkle et al. (2000), following the approach of Bruntt et al. (2008). The results for CoRoT-5 are shown in Table 2. Using these parameters for the atmospheric model, we determined the abundances of 21 individual elements. The uncertainty on the abundances includes a contribution of 0.04 dex due to the uncertainty on the fundamental parameters. The abundance pattern is shown in Fig. 4. The overall metallicity is found as the mean abundance of the elements with at least 20 lines (Si, Ca, Ti, Cr, Fe, Ni) giving $[M/H] = -0.25$±0.04. We did not include Mn, as this has a significantly lower abundance. The metallicity and the 1-σ error bar is indicated by the horizontal bar in Fig. 4. There is no evidence of the host star being chemically peculiar, except Mn.

The fundamental parameters of the parent star, its mass and radius were subsequently derived using stellar evolutionary tracks as presented in Deleuil et al. (2008) plotted in a $M^{(1/3)}/R$ - $T_{\rm eff}$ HR diagram. The stellar density parameter was derived from the lightcurve fitting (see sect. 7). We determined the mass and radius of the star to: $M_{\rm star} = 1.00$±0.02 $M_\odot$ and $R_{star} = 1.186$±0.04 $R_\odot$. As a final check, we calculated the corresponding surface gravity $\log g = 4.311$±0.033 while the spectroscopic value is 4.19 ± 0.03. These two values of $\log g$ are comparable with each other at the 3σ level. Based on our photometric analysis, we estimate the age of the star to 5.5 - 8.3 Gyrs. The spectra show no sign of Ca II emission or of a strong Li I absorption line, which is consistent with a relatively evolved star.

6. Period determination and transit timing variations

In total, 27 individual transit events are clearly seen, separated by an orbital period of about 4.03 days. One event was lost in a data gap.

First, we estimated the mid-times of each transit by applying the so-called Kwee-van Woerden method (Kwee & van Woerden 1956). This method mirrors the lightcurve around a pre-selected time-point, T, computes the differences of original and mirrored lightcurves and then searches for an optimum T. The $O-C$ diagram of the system was constructed, based on the resulting transit times and an initial guess of the period. A linear fit of this diagram yielded an improved estimate of the period. This period value was then refined with the following procedure. The lightcurve was phase-folded using this previously determined period and then averaged. The size of the bin used was 0.001 in phase (or to 5.81 minutes, using the final period). Then, this lightcurve was fitted (see the next section) by a theoretical transit lightcurve. The transit mid-times were then determined again by cross-correlating the observed and the theoretical lightcurve. This resulted in more precise mid-times of the transit and a new $O-C$ curve. Another linear fit to this $O-C$ diagram yielded a

Table 3. Parameters of the CoRoT-5 system derived from the combined MCMC analysis.

Fitted Parameters	Value	Units
$(R_p/R_{star})^2$	$0.01461^{+0.00030}_{-0.00032}$	
t_T	$0.0290^{+0.00038}_{-0.00053}$	
b	$0.755^{+0.017}_{-0.022}$	
K	$59.1^{+6.2}_{-3.1}$	$\mathrm{m\,s^{-1}}$
$e\cos\omega$	$-0.057^{+0.048}_{-0.020}$	
$e\sin\omega$	$-0.071^{+0.147}_{-0.130}$	

t_T denotes the transit duration given in fraction of phase, b the impact parameter and K the RV semi-amplitude.

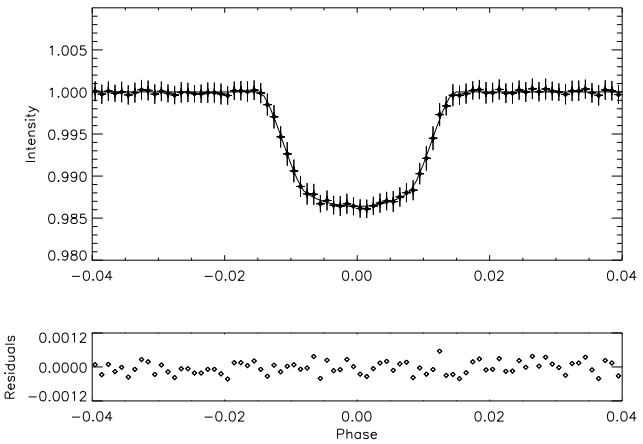

Fig. 6. Top: Phase-folded lightcurve of CoRoT-5b. Bottom: Residuals of fitted transit curve.

better period value, and the whole procedure was repeated. The final O-C diagram can be seen in Fig. 5. The resulting ephemeris is given in Table 4.

There is no obvious period variation present in the $O-C$ diagram. The first part of the lightcurve was obtained with the 512 sec sampling rate, so the first seven minima typically consist of only 20 data points. Thus, they have larger scatter and uncertainties. The next twenty minima were obtained with the high sampling rate (32 sec) and typically consist of a few hundred data points, leading to much higher accuracy. If one takes only these high-resolution minima into account, the constancy of the period is clearer. However, we cannot exclude that small period variations are present in the system. The upper limit of such a period variation was estimated by a quadratic fit to the data, which showed that it should be less than 0.42 seconds/cycle.

7. Analysis of parameters of CoRoT-5b

The final phase-folded lightcurve of the transit event is seen in Fig. 6. The transit signal shows a depth of about 1.4 % and lasts for about 2.7 hours. We derived the planetary parameters by fitting simultaneously the lightcurve of CoRoT-5 with the SOPHIE and HARPS radial velocities. A planetary model on a Keplerian orbit in the formalism of Giménez (2006a) and Giménez (2006b) was fitted to the data using a Markov Chain Monte-Carlo (MCMC) code described in Triaud et al. (in prep.) but using $e.\cos\omega$ and $e.\sin\omega$ instead of e and w as free parameters for better error estimation. In the fit a quadratic limb-darkening law was assumed at $u_+ = 0.616$ and $u_- = 0$. In the initial *burn-in* phase of the MCMC adjustment, 15,000 steps were chosen to allow the fit to converge. A further 50,000 steps were used to derive the best parameters and their errors. In the fit, there are eight fitted parameters plus two γ velocities and a normalization factor, totalling 11 free parameters. In addition, the fit assumed the presence of a Rossiter-McLaughlin effect with the two fixed parameters $vsin\,i = 1.0$ km s^{-1} and $\lambda = 0$ (λ: angle between stellar rotation axis and normal vector of the orbital plane). A Bayesian penalty is added to the χ^2 creating a prior for $M_\star = 0.99 \pm 0.02$. The fit to the rv measurements is shown in Fig. 2, and the derived fitting parameters are shown in Table 3.

In addition, a model transit curve (Mandel & Agol 2002) was fitted to the photometric phase folded transit curve separately. The parameters fitted are the center of transit, the planet radius expressed in stellar radii, the semi-major axis in stellar radii and the orbital inclination. In this fit the limb-darkening coefficients (u_1 and u_2) were free parameters, assuming a quadratic limb-darkening law. The fitting method follows a Metropolis-Hastings algorithm, which is a kind of Markov Chain Monte-Carlo procedure. The fitting procedure was performed ten times with different starting values to find the global minimum in χ^2. The errors of the fit were estimated from the standard deviations of the points in the chain. In addition to the transit curve, a third light component is included as a free parameter in the fit. In this way, we could check whether another contaminant is present, which remained unresolved in the photometric follow-up. However, no such additional source of light was found. The transformation between contamination factor c and the third light l_3 is $c = l_3/(1 - l_3)$. We had $c = 0.005 \pm 0.024$. Since we already removed the known contaminant factor from the lightcurve (see Section 2), we could therefore conclude that no further observable contaminant is present in the lightcurve of CoRoT-5. The planet parameters derived from this fit agree with the simultaneous fitting within the error bars, so we do not report them again here.

The resulting planetary parameters based on the MCMC approach with fixed limb-darkening coefficients and without any third light are summarized in Table 4. The major uncertainties on the planet are, as usual, introduced mainly from the uncertainty of the stellar parameters.

8. Summary

We report the discovery of a "hot-Jupiter-type" planet, CoRoT-5b, orbiting a type F9V star of 14.0 mag. The planet mass and radius were derived to $0.467^{+0.047}_{-0.024}$ M_{Jup} and $1.388^{+0.046}_{-0.047}$ R_{Jup}, respectively. It orbits its central star at $0.04947^{+0.00026}_{-0.00029}$ AU orbital distance. The determined eccentricity is low (see Table 4), but further radial velocity measurements would be needed for a more accurate determination.

CoRoT-5b has a density of $0.217^{+0.031}_{-0.025}$ g cm^{-3}, similar to the planets WASP-12b and WASP-15b (Hebb et al. 2009; West et al. 2009), implying that it belongs to the planets with the lowest mean density found so far. As

Table 4. The derived planet parameters.

Derived physical parameters	Value	Units
Transit epoch T_0	2454400.19885 ± 0.0002	HJD
Orbital period P	4.0378962 ± 0.0000019	days
Orbital semi-major axis a	$0.04947^{+0.00026}_{-0.00029}$	AU
Orbital inclination i	$85.83^{+0.99}_{-1.38}$	degrees
Orbital eccentricity e	$0.09^{+0.09}_{-0.04}$	
Argument of periastron ω	$-2.24^{+5.05}_{-0.84}$	rad
Planet radius $R_{\rm p}$	$1.388^{+0.046}_{-0.047}$	$R_{\rm J}$
Planet mass $M_{\rm p}$	$0.467^{+0.047}_{-0.024}$	$M_{\rm J}$
Mean planet density $\rho_{\rm p}$	$0.217^{+0.031}_{-0.025}$	gcm^{-3}
Planetary surface gravity $\log g_{\rm p}$	$7.77^{+0.14}_{-0.08}$	cgs
Zero albedo equilibrium temperature T_{eq}	1438 ± 39	K

such, it is found to be larger by 20% than standard evolution models (Guillot et al. 2006) would predict. Standard recipes that account for missing physics (kinetic energy transport or increased opacities) can explain this large size, and predict that the planet is mostly made of hydrogen-helium, with at most 28 $M_\oplus$ of heavy elements (maximum value obtained in the kinetic energy model, assuming 0.5% of the incoming energy is dissipated at the planet center). Thus, CoRoT-5b supports the proposed link between the metallicity of planets and of their host star.

Acknowledgements

HJD and JMA acknowledge support from grant ESP2007-65480-C02-02 of the Spanish Education and Science Ministry. Some of the data published in this article were acquired with the IAC80 telescope operated by the Instituto de Astrofísica de Tenerife at the Observatorio del Teide. The German CoRoT Team (TLS and Univ. Cologne) acknowledges DLR grants 50OW0204, 50OW0603, 50QP07011. RA acknowledges support by grant CNES-COROT-070879. The building of the input *CoRoT*/Exoplanet catalog was made possible by observations collected for years at the Isaac Newton Telescope (INT), operated on the island of La Palma by the Isaac Newton group in the Spanish Observatorio del Roque de Los Muchachos of the Instituto de Astrofisica de Canarias.

References

Aigrain, S., Collier Cameron, A., Ollivier, M., et al. 2008, A&A, 488, L43
Alonso, R., Auvergne, M., Baglin, A., et al. 2008, A&A, 482, L21
Auvergne, M., Bodin, P., Boisnard, L., et al. 2009, ArXiv e-prints
Baglin, A., Auvergne, M., Barge, P., et al. 2007, in American Institute of Physics Conference Series, Vol. 895, American Institute of Physics Conference Series, ed. C. Dumitrache, N. A. Popescu, M. D. Suran, & V. Mioc, 201–209
Baranne, A., Queloz, D., Mayor, M., et al. 1996, A&AS, 119, 373
Barge, P., Baglin, A., Auvergne, M., et al. 2008, A&A, 482, L17
Boisnard, L., Baglin, A., Auvergne, M., Deleuil, M., & Catala, C. 2006, in ESA Special Publication, Vol. 1306, ESA Special Publication, 465–471
Bouchy, F., Queloz, D., Deleuil, M., et al. 2008, A&A, 482, L25
Bruntt, H., Catala, C., Garrido, R., et al. 2002, A&A, 389, 345
Bruntt, H., De Cat, P., & Aerts, C. 2008, A&A, 478, 487
Deleuil, M., Deeg, H. J., Alonso, R., et al. 2008, A&A, 491, 889
Deleuil, M., Meunier, J. C., Moutou, C., et al. 2009, AJ, 138, 649
Frasca, A., Alcalá, J. M., Covino, E., et al. 2003, A&A, 405, 149
Gandolfi, D., Alcalá, J. M., Leccia, S., et al. 2008, ApJ, 687, 1303
Giménez, A. 2006a, A&A, 450, 1231
Giménez, A. 2006b, ApJ, 650, 408
Guillot, T., Santos, N. C., Pont, F., et al. 2006, A&A, 453, L21
Hebb, L., Collier-Cameron, A., Loeillet, B., et al. 2009, ApJ, 693, 1920
Heiter, U., Kupka, F., van't Veer-Menneret, C., et al. 2002, A&A, 392, 619
Hinkle, K., Wallace, L., Valenti, J., & Harmer, D. 2000, Visible and Near Infrared Atlas of the Arcturus Spectrum 3727-9300 A (Visible and Near Infrared Atlas of the Arcturus Spectrum 3727-9300 A ed. Kenneth Hinkle, Lloyd Wallace, Jeff Valenti, and Dianne Harmer. (San Francisco: ASP) ISBN: 1-58381-037-4, 2000.)
Kupka, F., Piskunov, N., Ryabchikova, T. A., Stempels, H. C., & Weiss, W. W. 1999, A&AS, 138, 119
Kwee, K. K. & van Woerden, H. 1956, Bull. Astron. Inst. Netherlands, 12, 327
Llebaria, A., Guterman, P., & Ollivier, M. 2003, in Techniques and Instrumentation for Detection of Exoplanets. Edited by Coulter, Daniel R. Proceedings of the SPIE, Volume 5170, pp. 155-166 (2003)., 155–166
Mandel, K. & Agol, E. 2002, ApJ, 580, L171
Mayor, M., Pepe, F., Queloz, D., et al. 2003, The Messenger, 114, 20
Michel, E., Deleuil, M., & Baglin, A. 2006, in ESA Special Publication, Vol. 1306, ESA Special Publication, ed. M. Fridlund, A. Baglin, J. Lochard, & L. Conroy, 473–+
Moutou, C., Bruntt, H., Guillot, T., et al. 2008, A&A, 488, L47
Pepe, F., Mayor, M., Queloz, D., et al. 2005, The Messenger, 120, 22
Pinheiro da Silva, L., Rolland, G., Lapeyrere, V., & Auvergne, M. 2008, MNRAS, 384, 1337
Queloz, D., Henry, G. W., Sivan, J. P., et al. 2001, A&A, 379, 279
Quentin, C., Barge, P., Cautain, R., et al. 2006, in ESA Special Publication, Vol. 1306, ESA Special Publication, 409–+
Santos, N. C., Mayor, M., Naef, D., et al. 2002, A&A, 392, 215
Surace, C., Alonso, R., Barge, P., et al. 2008, in Society of Photo-Optical Instrumentation Engineers (SPIE) Conference Series, Vol. 7019, Society of Photo-Optical Instrumentation Engineers (SPIE) Conference Series
Valenti, J. A. & Piskunov, N. 1996, A&AS, 118, 595
West, R. G., Anderson, D. R., Gillon, M., et al. 2009, AJ, 137, 4834

[1] Institute of Planetary Research, DLR, Rutherfordstr. 2, 12489 Berlin, Germany
[2] Center for Astronomy and Astrophysics, TU Berlin, Hardenbergstr. 36, 10623 Berlin, Germany
[3] Observatoire de Genève, Universite de Genève, 51 Ch. des Maillettes, 1290 Sauverny, Switzerland
[4] Laboratoire d'Astrophysique de Marseille, CNRS UMR 6110, Traverse du Siphon, 13376 Marseille, France

[5] School of Physics, University of Exeter, Stocker Road, Exeter EX4 4QL, United Kingdom
[6] Instituto de Astrofsica de Canarias, E-38205 La Laguna, Tenerife, Spain
[7] LESIA, CNRS UMR 8109, Observatoire de Paris, 5 place J. Janssen, 92195 Meudon, France
[8] Institut d'Astrophysique de Paris, UMR7095 CNRS, Universite Pierre & Marie Curie, 98bis Bd Arago, 75014 Paris, France
[9] Sydney Institute for Astronomy, School of Physics, University of Sydney, NSW 2006, Australia
[10] Rheinisches Institut für Umweltforschung an der Universität zu Köln, Abt. Planetenforschung, Aachener Str. 209, 50931 Köln, Germany
[11] Research and Scientific Support Department, European Space Agency, ESTEC, 2200 Noordwijk, The Netherlands
[12] Institute for Astronomy, University of Vienna, Türkenschanzstrasse 17, 1180 Vienna, Austria
[13] Observatoire de la Côte d'Azur, Laboratoire Cassiopée, CNRS UMR 6202, BP 4229, 06304 Nice Cedex 4, France
[14] Thüringer Landessternwarte Tautenburg, Sternwarte 5, 07778 Tautenburg, Germany
[15] Space Research Institute, Austrian Academy of Sciences, Schmiedlstrasse 6, 8042 Graz, Austria
[16] Institut d'Astrophysique Spatiale, Université Paris XI, 91405 Orsay, France
[17] LUTH, Observatoire de Paris-Meudon, 5 place J. Janssen, 92195 Meudon, France
[18] Institut dAstrophysique et de Géophysique, Université de Liège, Allée du 6 aout 17, Sart Tilman, Liège 1, Belgium
[19] Observatorio Nacional, Rio de Janeiro, RJ, Brazil
[20] School of Physics and Astronomy, Raymond and Beverly Sackler Faculty of Exact Sciences, Tel Aviv University, Tel Aviv 69978, Israel